TGF-β1 modulates microglial phenotype and promotes recovery after intracerebral hemorrhage

Roslyn A. Taylor,[1,2] Che-Feng Chang,[1] Brittany A. Goods,[3] Matthew D. Hammond,[1,4] Brian Mac Grory,[1] Youxi Ai,[1] Arthur F. Steinschneider,[1] Stephen C. Renfroe,[1] Michael H. Askenase,[1] Louise D. McCullough,[4,5] Scott E. Kasner,[6] Michael T. Mullen,[6] David A. Hafler,[1] J. Christopher Love,[7] and Lauren H. Sansing[1]

[1]Department of Neurology, Yale School of Medicine, New Haven, Connecticut, USA. [2]Department of Immunology, University of Connecticut Health, Farmington, Connecticut, USA. [3]Department of Biological Engineering, Koch Institute for Integrative Cancer Research at Massachusetts Institute of Technology, Cambridge, Massachusetts, USA. [4]Department of Neuroscience, University of Connecticut Health, Farmington, Connecticut, USA. [5]Department of Neurology, McGovern Medical School, University of Texas Health Science Center at Houston, Houston, Texas, USA. [6]Department of Neurology, University of Pennsylvania Perelman School of Medicine, Philadelphia, Pennsylvania, USA. [7]Department of Chemical Engineering, Koch Institute for Integrative Cancer Research, Massachusetts Institute of Technology, Cambridge, Massachusetts, USA.

Intracerebral hemorrhage (ICH) is a devastating form of stroke that results from the rupture of a blood vessel in the brain, leading to a mass of blood within the brain parenchyma. The injury causes a rapid inflammatory reaction that includes activation of the tissue-resident microglia and recruitment of blood-derived macrophages and other leukocytes. In this work, we investigated the specific responses of microglia following ICH with the aim of identifying pathways that may aid in recovery after brain injury. We used longitudinal transcriptional profiling of microglia in a murine model to determine the phenotype of microglia during the acute and resolution phases of ICH in vivo and found increases in TGF-β1 pathway activation during the resolution phase. We then confirmed that TGF-β1 treatment modulated inflammatory profiles of microglia in vitro. Moreover, TGF-β1 treatment following ICH decreased microglial *Il6* gene expression in vivo and improved functional outcomes in the murine model. Finally, we observed that patients with early increases in plasma TGF-β1 concentrations had better outcomes 90 days after ICH, confirming the role of TGF-β1 in functional recovery from ICH. Taken together, our data show that TGF-β1 modulates microglia-mediated neuroinflammation after ICH and promotes functional recovery, suggesting that TGF-β1 may be a therapeutic target for acute brain injury.

Introduction

Intracerebral hemorrhage (ICH) is a subtype of stroke that results from the rupture of a blood vessel within the brain parenchyma, often due to hypertension (1). ICH has a high mortality rate; 40%–50% of patients die within the first 30 days. Currently, there is no specific treatment for ICH (1, 2). The exposure of brain tissue to blood components results in activation of microglia, the tissue-resident macrophages of the central nervous system, and the recruitment of peripheral leukocytes to the perihematomal region (3). This early activation of the immune system leads to secondary injury after ICH. Activated microglia and peripheral leukocytes secrete proinflammatory cytokines, ROS, and matrix metalloproteinases, which contribute to blood-brain barrier breakdown and neuronal injury (3). Microglia and blood-derived macrophages, however, can phagocytose the hematoma, resulting in decreased gene expression of *Il1b*, *Tnf*, and matrix metalloproteinase 9 (*Mmp9*) (4). The signals that aid in the transition to the resolution of inflammation are currently unknown and represent an important therapeutic target for ICH treatment.

Microglia are often studied in conjunction with peripheral macrophages that have infiltrated the brain parenchyma follow-

ing ICH due to the expression of similar surface markers. It has recently been shown, however, that unlike blood-derived macrophages, microglia derive from yolk sac erythromyeloid progenitors. Microglia develop independently of the transcription factor c-Myb and hematopoietic stem cells (5, 6) but are dependent upon the transcription factors IRF8 and PU.1 (7). Microglia also have a unique molecular signature that is distinct from that of blood-derived macrophages (8, 9). These signatures indicate that microglia and blood-derived macrophages likely play distinct roles in disease pathogenesis and recovery — hence the need to study these populations independently.

Tissue-resident macrophages often have prominent roles in organ development and homeostasis (10). Indeed, it has recently become appreciated that microglia prune neural synapses, guiding the development and maintenance of neural networks in the brain (11). As the predominant immune population in the central nervous system, microglia are poised to be the first responding cells at the site of injury and infection, as well as to aid in tissue repair (12, 13). In an autologous blood murine model of ICH, microglial activation occurs as early as 4 hours after ICH and can persist for up to 4 weeks (14). Microglial activation results in diverse phenotypic profiles that have been historically simplified as classical or alternative forms of activation. In models of neuroinflammation, classically activated microglia have been associated with proinflammatory cytokine production and secretion of inducible nitric

oxide species (15). Alternatively activated microglia secrete antiin-flammatory cytokines and neurotrophic factors, and are associated with wound healing and repair (12, 16).

Microglial alternative activation is commonly attributed to IL-4/IL-13 signaling through STAT6 (16, 17). In the experimental autoimmune encephalomyelitis (EAE) murine models of multiple sclerosis, mice with a CNS IL-4 deficiency had exacerbated disease and reduced microglial YM1, a marker of alternative activation (18). IL-4 deficiency resulted in an increase in proinflammatory gene expression, larger infarcts, and worse functional outcomes 20 days after ischemic stroke (19). IL-10 induces macrophage alternative activation (20) and induces SOCS3 to downregulate inflammation in macrophages and microglia (21), and overexpression of IL-10 improves stroke outcomes (22). TGF-β1 has been recently shown to play a pivotal role in microglial development and homeostasis both in vitro and in vivo (8) and is also capable of inducing wound healing responses in macrophages through SMAD2 and SMAD3 signaling pathways (20, 23, 24). Given the potential for microglia to aid in recovery after brain injury and the recently identified unique spectrum of microglial responses (25), we aimed to determine the activation profiles of microglia during the acute inflammatory and resolution phases after ICH and to determine the mediator(s) of the activation of microglia during recovery. Using transcriptional profiling, we identified a molecular signature that characterizes resolution phase of perihematomal microglia. We additionally identified TGF-β1 as the most likely mediator. We then confirmed the benefit of TGF-β1 in reducing microglial inflammatory cytokine and chemokine expression both in vitro and in vivo. Finally, we found that patients with an increased TGF-β1 response during the first few days after ICH had improved long-term outcomes even after adjusting for ICH severity. Taken together, our results identify TGF-β1 as the likely mediator of a reparative phenotype in microglia and critical to recovery after ICH.

Results

The perihematomal region transitions from proinflammatory to antiinflammatory within the first 2 weeks after ICH. We first sought to determine the cytokines and chemokines present in the perihematomal region over the first 2 weeks after ICH in order to identify both the factors that could influence microglial polarization and the changes in the brain milieu that could be attributed to microglial activation. According to multiplexed ELISA analysis on brain tissue homogenate, concentrations of the proinflammatory cytokine IL-6 were elevated 1 and 3 days after ICH and subsequently rapidly decreased (Figure 1A). CCL2 and IL-17 were elevated in the perihematomal region at 3 days and then decreased. There were no changes in IFN-γ or IL-10. IL-4 was undetectable in the perihematomal region at all time points measured, while IL-13 increased from baseline to day 3. In contrast, TGF-β1 and brain-derived neurotrophic factor (BDNF), factors associated with resolution of inflammation and neurogenesis, increased from day 1 to day 10 and remained elevated at 14 days. Our data indicate that the proinflammatory perihematomal brain environment is characterized by IL-6, CCL2, and IL-17 during the first 3 days. This milieu changes dramatically toward recovery within the first 2 weeks after ICH.

Microglial phenotypes transition from a proinflammatory phenotype to an antiinflammatory phenotype a week after ICH. We

hypothesized that the changes to the cytokine milieu of the perihematomal region after ICH reflected changes to the activation statuses of microglia in this region. Thus, we investigated the phenotypic changes specifically in microglia over time after ICH. We sorted microglia from perihematomal regions in order to study changes in microglial gene expression (Figure 1B). At 12 hours, microglial *Il6* gene expression was markedly elevated; however, this was transient, and expression decreased dramatically by 24 hours and then remained low through day 14. Microglia also had elevated *Ccl2* gene expression early in the first week that decreased by 14 days (Figure 1C).

In order to obtain a more complete understanding of changes in microglial gene expression after ICH, we performed a transcriptional analysis of 780 genes from microglia sorted from mouse brains over the course of 28 days. Overall, the largest changes in gene expression occurred between days 3 and 7 (Supplemental Figure 1A, clusters enlarged in Supplemental Figure 1, B–F; supplemental material available online with this article; doi:10.1172/JCI88647DS1). Principal components analysis (PCA) identified 78 genes that accounted for the greatest variability in microglial gene expression over the time course. Replicate samples separated consistently according to time point, indicating that PCA revealed distinct temporal patterns in gene expression by identifying genes that contribute to the variance across time (Figure 2A, annotated in Supplemental Figure 1G). Hierarchical clustering of these 78 genes across samples is shown in the heat map and shows clear patterns of transcription and groupings of samples by time point (Figure 2B). The top cluster identifies a set of genes that has low expression in naive microglia but high expression at day 1 after ICH. These genes include *Ly86*, *Cxcl10*, *Tnf*, *Tlr7*, *Lcp1*, and *Itga6*, indicating an activated, proinflammatory phenotype. Microglia then downregulate these genes by day 3. At day 3, the peak of peripheral leukocyte recruitment, microglia express high levels of several chemokines and cytokines, including *Ccl4*, *Ccl3*, *Cd14*, *Cd83*, *Il1a*, and *Tnfaip3*. Several lower clusters identify genes with low expression days 1–3 after ICH, with increased expression beginning on day 7 and continuing throughout the recovery phase. These genes provided evidence of ongoing inflammation, such as *Il6ra*, *Fcgr1*, and *Irf5*. However, beginning in this period we observed upregulation of *Tgfbr1*, *Tgfbr2*, and *Tgfb1*, as well as genes associated with cell adhesion and phagocytosis (*Cd164* and *Lamp1*) and the inhibition of T cell activation (*Lag3*). We used genes that contributed most to this recovery phase phenotype in our PCA to perform GO functional enrichment analysis. We found that TGF-β receptor binding and signaling pathways were significantly enriched, as well as wound healing functions (Figure 2C). Displaying these genes as a network, we also found that these genes were highly coexpressed and had many physical interactions (Figure 2D). Taken together, our results have identified a set of gene modules driven by TGF-β signaling that characterize microglia in repair and recovery.

Through the canonical signaling pathway, TGF-β1 signals via phosphorylation of SMAD2 and SMAD3 proteins (26). Brain sections from WT mice at 14 days showed CD11b⁺pSMAD2⁺ cells in the perihematomal region (Supplemental Figure 2A). At this time point, the majority of the blood-derived monocytes had left the perihematomal region, suggesting that the CD11b⁺pSMAD2⁺
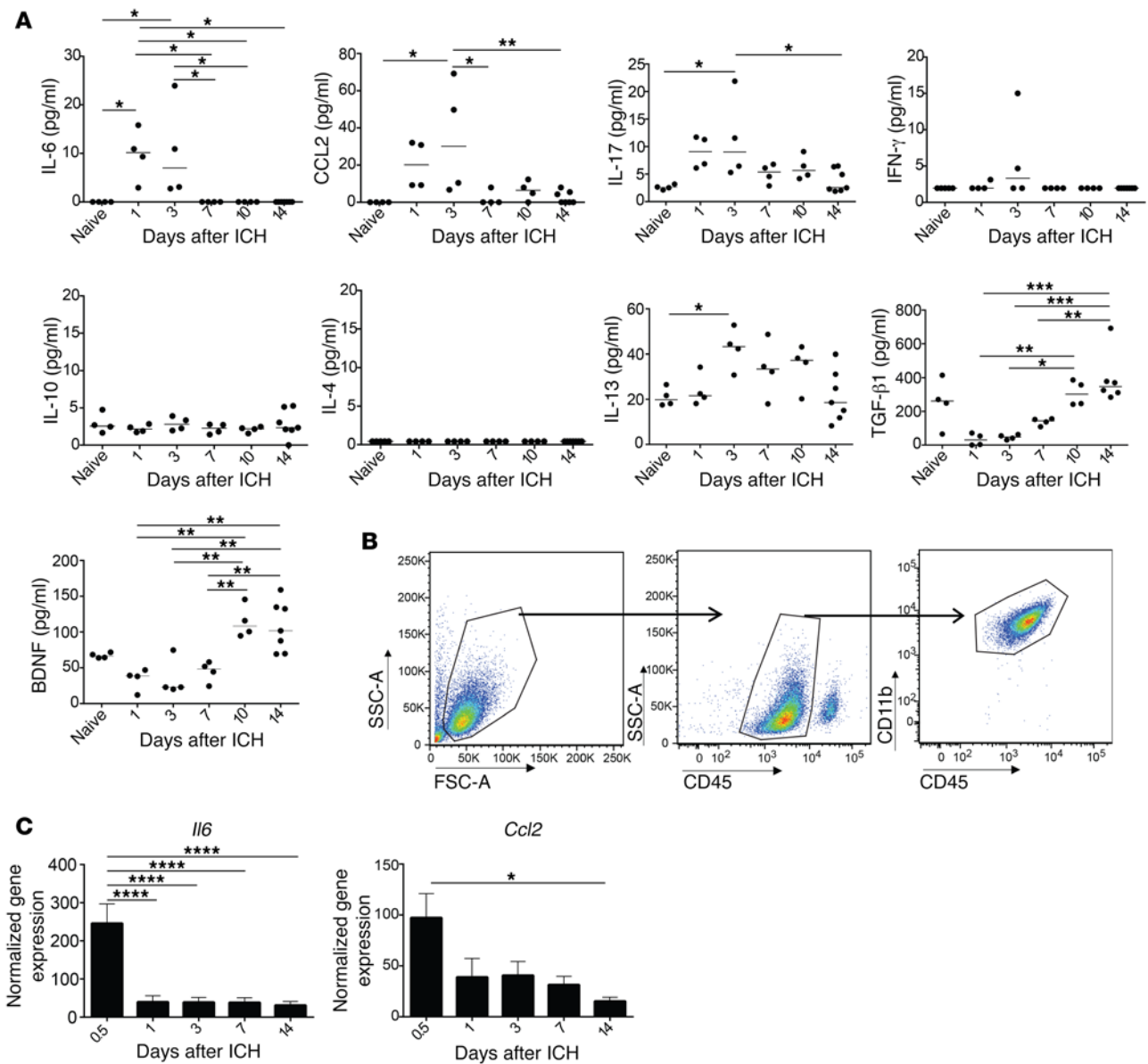
Figure 1. Microglia downregulate proinflammatory genes by 7 days after ICH. (**A**) Multiplex assays (IL-6, CCL2, IL-17, IFN-γ, IL-10, IL-4, IL-13) and ELISA assays (TGF-β1 and BDNF) were performed on brain tissue homogenates of the perihematomal regions of WT mice at baseline and 1, 3, 7, 10, and 14 days after ICH. Individual mice represented as one dot with the line at the median value. n = 4–7 mice/time point. (**B**) Gating strategy to isolate microglia for cell sorting experiments. Samples were gated on live singlets prior to leukocytes being found by forward and side scatter. Samples were then gated on side scatter, CD45int to separate microglia from peripheral leukocytes and then on CD45int, CD11b+ to obtain microglia. (**C**) qRT-PCR for *Il6* and *Ccl2* was performed on cell-sorted microglia from CX3CR1-heterozygous mice at baseline, 12 hours, and 1, 3, 7, and 14 days after ICH. Means graphed with SEM; n = 7–16. Results in **A** and **C** were analyzed by ANOVA followed by Tukey's post hoc test; *P < 0.05, **P < 0.01, ***P < 0.001, ****P < 0.0001.

cells were likely microglia. In contrast, we did not find evidence that astrocytes were responding to TGF-β1 at this time point (Supplemental Figure 2B).

Alternative microglial activation has historically been associated with IL-4 and IL-13 signaling (15). We did find evidence of increased IL-13 in the brain (Figure 1A). Nonetheless, microglial gene expression of *Il4Ra*, the receptor for both cytokines, was not upregulated over time. Furthermore, we found no evidence for phosphorylation of STAT6 in microglia (Supplemental Figure 2C). Our data suggest that IL-4 and IL-13 do not mediate a traditionally defined alternatively activated phenotype in microglia after ICH.

Instead, these data show that microglia are both producing and signaling through TGF-β1 during the second week after ICH, suggesting that TGF-β1 may have a role in microglia-mediated recovery.

Mice with dysregulated microglia fail to upregulate Tgfb1 gene expression and have worse functional outcomes after ICH. Microglia express the chemokine receptor CX3CR1 under homeostatic conditions (27). Its ligand, CX3CL1, is constitutively expressed by neurons and can either be membrane bound or secreted as a chemokine (28). Binding of microglial CX3CR1 to neuronal CX3CL1 maintains microglial quiescence (29, 30), and in animal models of LPS-induced neuroinflammation, ALS, and Parkinson's
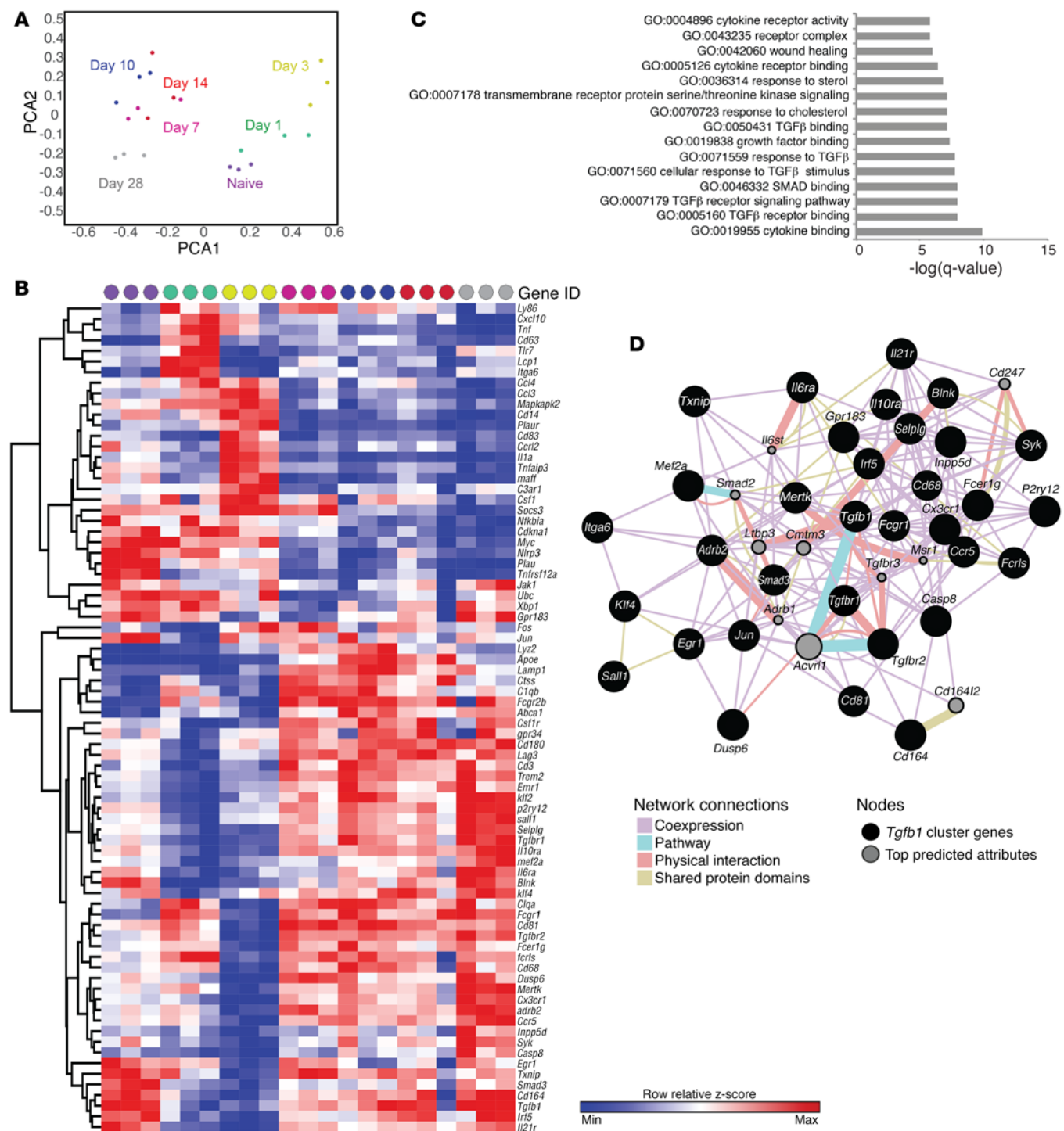
Figure 2. Temporal transcriptional analysis of microglia after ICH. (**A**) Scatter plots show each sample projected on the first two principal components and are color coded according to time point. Biological replicates cluster closely at each time point. (**B**) Heatmap of the *Z* score of genes identified by PCA for each sample. Data were clustered hierarchically in GENE-E using one minus Pearson correlation and complete linkage. Data are colored according to row minimum and maximum. Time points are color coded as in **A**, and days 10–28 cluster most closely. Each replicate includes microglia from 3 brains, and there are 3 biological replicates per time point. (**C**) GO biological process enrichment analysis was performed using genes appearing in the resolution phase quadrant of the PCA. TGF-β1 pathways account for the majority of the top 15 GO functions. (**D**) The network diagram shows each gene identified in the resolution phase, including TGF-β1, as a node, and connections are indicated by function.
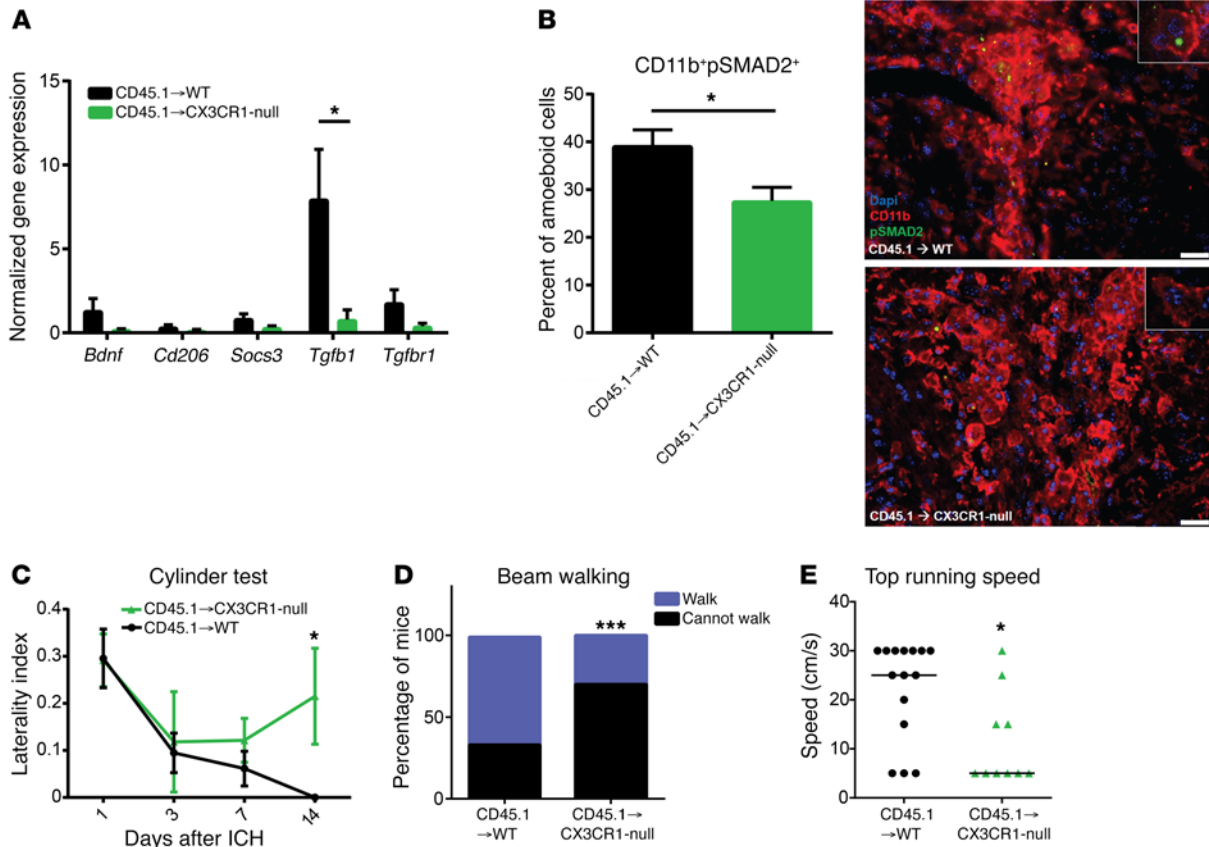
Figure 3. Microglial alternative activation is required for functional recovery after ICH. (**A**) Microglia were cell sorted from WT and CX3CR1-null BM chimeras 14 days after ICH and then processed for qRT-PCR. CX3CR1-null microglia have a significant reduction in TGF-β1 gene expression compared with WT microglia. Means graphed with SEM; Student's *t* test; *n* = 7–9. (**B**) Brain sections from WT and CX3CR1-null BM chimeras were stained for CD11b (red) and pSMAD2 (green) 14 days after ICH. Nuclei were stained with DAPI. ×40 images, with inset at ×64. Scale bars: 25 μm. Quantification of percent of pSMAD2⁺, amoeboid CD11b⁺ graphed as mean with SD; Student's *t* test; *n* = 4. (**C**) BM chimeras were cylinder tested 1, 3, 7, and 14 days after ICH. CX3CR1-null chimeras maintain a right forelimb preference 14 days after ICH. Means graphed with SEM. Repeated measures ANOVA followed by Tukey's post hoc test; *n* = 10–12. (**D**) Beam walking test shows that CX3CR1-null BM chimeras do not walk as well on the beam 14 days after ICH. Percentage of mice able versus unable to walk is graphed. Wilcoxon rank sum test; *n* = 11–13. (**E**) Forced run test shows that CX3CR1-null BM chimeras do not run as quickly as WT BM chimeras 14 days after ICH. Individual dots represent individual mice, with line at the median; Mann-Whitney *U* test, *n* = 10–15. *$P < 0.05$, ***$P < 0.001$.

disease, CX3CR1-null mice have worse functional outcomes and elevated levels of IL-1β after LPS-mediated neuroinflammation (30, 31). We therefore utilized the CX3CR1 regulation of microglial phenotype as a model system for studying the microglial responses in recovery after ICH.

Monocytes and several other leukocyte populations also express CX3CR1. In order to study CX3CR1 on microglia specifically, we made bone marrow (BM) chimeras using WT and CX3CR1-null mice as hosts and congenically marked WT BM as the donor (Supplemental Figure 3A). As microglia are radioresistant and should remain of host origin after irradiation (32), this experimental design allows for comparison of WT and CX3CR1-null microglia after ICH in mice with an otherwise WT immune compartment. CX3CR1-null microglia had a significant reduction in TGF-β1 gene expression at 14 days compared with WT microglia. Differences between the genotypes were not observed in microglial gene expression of alternatively activated markers *Bdnf*, *Socs3*, *Cd206* (*Mrc1*), or *Tgfbr1* (Figure 3A). We examined the perihematomal region by immunofluorescence and found that the WT BM chimeras had a very contracted region of amoeboid CD11b⁺ cells

around the minimal residual hemorrhage with obvious costaining of pSMAD2 at 14 days. In contrast, the CX3CR1-null BM chimeras had a more widespread region of activated CD11b⁺ cells and many fewer CD11b⁺pSMAD2⁺ cells in the perihematomal region (Figure 3B). These findings indicate that in the absence of CX3CR1 signaling, the microglia do not modulate the phenotype to either produce or signal through TGF-β1 in the recovery phase of ICH.

We next performed behavioral tests on WT and CX3CR1-null BM chimeras to determine whether there is a functional consequence to failing to modulate microglial phenotype. There were no behavioral differences between naive WT and CX3CR1-null BM chimeras on cylinder and beam walking tests (Supplemental Figure 3, B and C), indicating no baseline functional effect of lacking microglial expression of CX3CR1. After ICH, the two genotypes had similar weight loss at 24 hours and displayed equal neurological deficits at 24 and 72 hours (Figure 3C and Supplemental Figure 3D), suggesting microglial CX3CR1 does not impact acute inflammation. Consistent with the reduction in TGF-β1 signaling during the recovery phase, the CX3CR1-null BM chimeras exhibited a right forelimb preference, showing a left hemiparesis, impaired
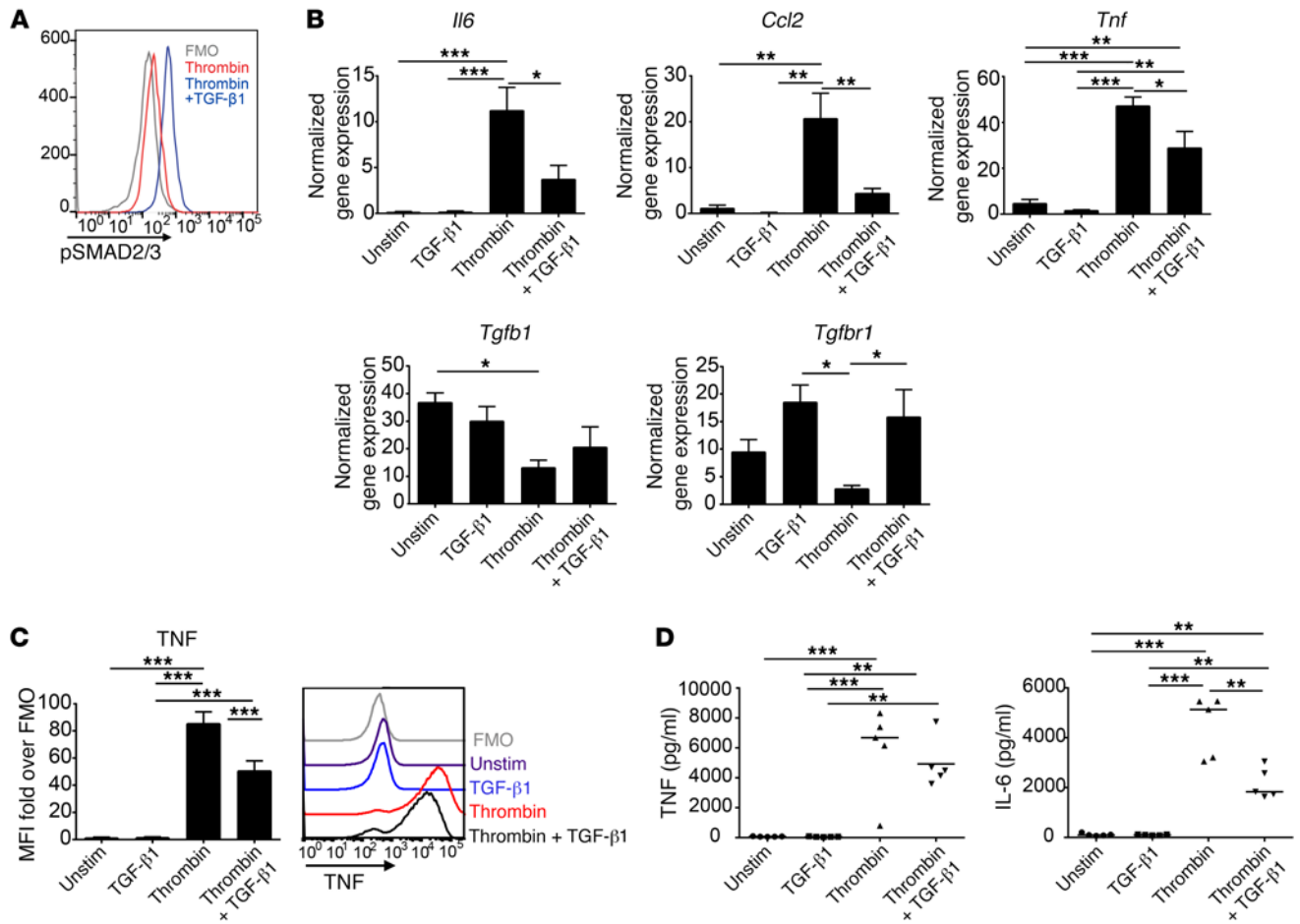
Figure 4. TGF-β1 modulates microglia-mediated neuroinflammation in vitro. (**A**) Primary microglia respond to TGF-β1 treatment and signal through pSMAD2/3 after 15 minutes of stimulation in vitro. Representative histogram shown with fluorescence minus one (FMO) (gray), thrombin treated (red), and thrombin + TGF-β1 (blue); *n* = 3. (**B**) Thrombin + TGF-β1–treated microglia have a reduction in *Il6*, *Ccl2*, and *Tnf* gene expression and an increase in *Tgfbr1* gene expression compared with microglia treated with thrombin alone after 8 hours of stimulation. Means graphed with SEM. *n* = 5 individual experiments with 3 technical replicates per group, per experiment. unstim, unstimulated. (**C**) Microglia treated with thrombin + TGF-β1 have reduced TNF production after 8 hours of stimulation. Means graphed with SEM. Representative histograms show FMO (gray), unstimulated (purple), TGF-β1 alone (blue), thrombin (red), and thrombin + TGF-β1 (black). *n* = 8. (**D**) TNF and IL-6 ELISA on cell supernatants taken after 24 hours of stimulation. Individual wells are represented by dots, with line at the median; *n* = 5. All statistical analysis performed by ANOVA, followed by Tukey's post hoc test. *$P < 0.05$, **$P < 0.01$, ***$P < 0.001$.

beam walking, and slower top running speeds at 14 days after ICH (Figure 3, C–E). Our data suggest that microglial CX3CR1 signaling on microglia is required for phenotype modulation and functional recovery after ICH and support the hypothesis that TGF-β1 mediates microglial alternative activation.

TGF-β1 modulates microglia-mediated neuroinflammation in vitro. In order to directly measure the effects of TGF-β1 on microglia, we next determined whether TGF-β1 modulates microglia-mediated neuroinflammation in vitro. Activated primary microglia respond to TGF-β1 in vitro, as indicated by an increase in pSMAD2/3 (Figure 4A). Thrombin is a serine protease activated during coagulation, present at high levels in ICH, and is frequently used as the stimulus to mimic ICH in vitro (33, 34). Consistent with our in vivo results, stimulation of microglia with thrombin resulted in an upregulation of the genes *Il6*, *Tnf*, and *Ccl2*. These inflammatory responses were reduced by TGF-β1 (Figure 4B). Thrombin treatment also resulted in a reduction in *Tgfb1* and *Tgfbr1* gene expression; TGF-β1 treatment restored *Tgfbr1* gene expression.

The effects of thrombin and TGF-β1 were then confirmed at the protein level. After 8 hours of stimulation, intracellular cytokine staining showed that primary microglia activated with thrombin and TGF-β1 produced less TNF than those activated with thrombin alone (Figure 4C); ELISA of the cell culture supernatant likewise revealed decreased levels of IL-6 and TNF after treatment with TGF-β1 (Figure 4D).

TGF-β1 treatment reduced microglial inflammation and improves functional outcomes 24 hours after ICH. We next examined whether TGF-β1 induces a microglia phenotype that improves functional recovery after ICH. To specifically target the microglia in the perihematomal region, mice were initially pretreated with 10 ng TGF-β1 or vehicle intracerebrally immediately prior to subjecting the mice to ICH. Mice given TGF-β1 treatment had improved functional outcomes on cylinder test and the beam walking test at 24 hours (Supplemental Figure 4).

In order to test whether TGF-β1 can improve functional recovery after ICH in a more translationally relevant time frame, we
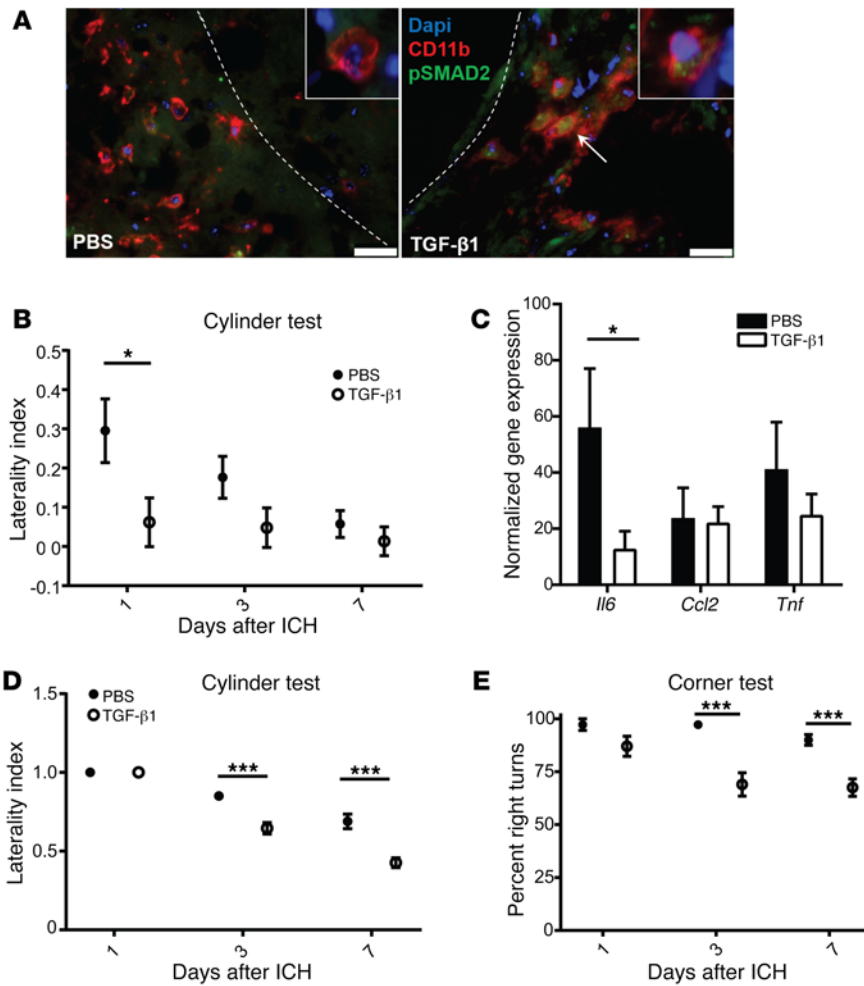
Figure 5. TGF-β1 treatment promotes better functional outcomes and modulates microglial IL-6 after ICH. (**A**) TGF-β1 treatment led to phosphorylation of SMAD2 in myeloid cells in the brain. Brain sections from PBS- or TGF-β1–treated mice were stained at 24 hours for CD11b (red) and pSMAD2 (green). Nuclei were stained with DAPI. Arrow indicates cluster of pSMAD2⁺CD11b⁺ cells. Dotted line depicts edge of hematoma. 40×, with inset at 64×. Scale bars: 25 μm. $n = 4$–5. (**B**) Cylinder test shows that TGF-β1–treated mice have better functional outcomes 24 hours after ICH. Repeated measures ANOVA, followed by a Tukey's post hoc test; $n = 11$–12. (**C**) TGF-β1–treated microglia have reduced *Il6* gene expression 24 hours after ICH. Means graphed with SEM; Student's *t* test; $n = 7$–9. (**D** and **E**) TGF-β1–mediated improvements in behavioral outcomes were confirmed using the collagenase model of ICH. Cylinder test (**D**) and corner test (**E**) show TGF-β1–treated mice have better functional outcomes at 3 and 7 days after ICH. Repeated measures ANOVA, followed by Tukey's post hoc test; $n = 9$–10. *$P < 0.05$, ***$P < 0.001$.

treated mice with either TGF-β1 or PBS intracerebroventricularly 4 hours after ICH. Confirming the feasibility of this approach, CD11b⁺pSMAD2⁺ cells were found in the perihematomal region of the TGF-β1–treated mice at 24 hours, a time point prior to the induction of the TGF-β1 pathway in untreated mice (Figure 5A). Mice treated with a single dose of TGF-β1 4 hours after ICH had completely recovered motor function at 24 hours (Figure 5B). This recovery persisted for at least 1 week. TGF-β1 treatment also significantly reduced ICH-induced microglial *Il6* gene expression (Figure 5C). We then confirmed this beneficial effect of TGF-β1 treatment in the collagenase model of ICH, which produces a more severe hemorrhage with prolonged functional recovery (35). Mice treated with a single dose of TGF-β1 had better functional outcomes by cylinder test (Figure 5D) and corner test (Figure 5E) at 3 and 7 days after ICH. We did not observe a difference between the treatment groups in microglial numbers at 24 hours, in iron-positive cells at day 7, or in leukocyte recruitment (Supplemental Figure 5). Overall, these data suggest that TGF-β1 targets microglia and improves behavioral outcomes independent of TNF, CCL2, leukocyte infiltration, and hematoma clearance.

TGF-β1 response is associated with improved outcomes at 90 days in patients with ICH. In the murine model, TGF-β1 levels were high in the naive state in both perihematomal brain tissue and in microglia, decreased acutely after ICH, and began to increase again around day 7. A similar trend was observed in circulating (peripheral) TGF-β1 levels over time in the mouse model (Supplemental Figure 6). In addition, administration of TGF-β1 at a time point earlier than TGF-β1 was normally induced led to improved outcomes in mice. Although there is no way to measure TGF-β1 levels in patients prior to their experiencing ICH, we hypothesized that patients would also have an acute reduction in TGF-β1 after ICH that would then recover. Furthermore, we hypothesized that earlier TGF-β1 recovery in the acute phase after ICH would be associated with better long-term outcomes in patients. We measured plasma TGF-β1 concentrations in patients at 6 and 72 hours after ICH in a prospective cohort study and in a cohort of control patients with similar ages and rates of hypertension, the primary risk factor for ICH. The clinical characteristics of the patients are shown in Supplemental Table 1. As expected, at 6 hours after ICH, the levels of TGF-β1 were lower than in the control cohort (ICH 315.9 pg/ml vs. control 841 pg/ml, $P < 0.001$) (Figure 6A).

Functional outcomes of patients were measured using the modified Rankin scale, the most commonly used scale to quantify disability after stroke (35, 36). Interestingly, about half of our patients had increased TGF-β1 levels from 6 to 72 hours (assumed to be early recovery of TGF-β1), while half had decreased TGF-β1 (prolonged suppression of TGF-β1) (Figure 6A). The two cohorts were balanced in age, sex, and stroke severity measures (Table 1).
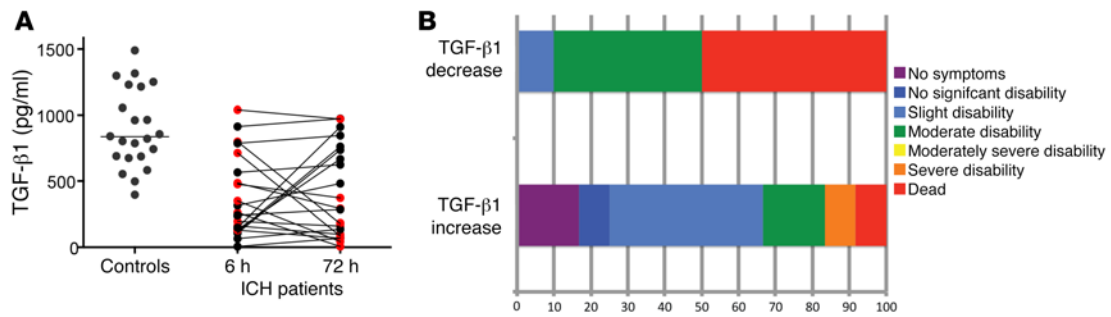
Figure 6. An increase in TGF-β1 plasma levels from 6 to 72 hours after ICH is independently associated with better patient outcomes at 90 days. Plasma TGF-β1 concentrations were measured from controls and ICH patients at 6 ± 6 and 72 ± 6 hours after onset of ICH. (**A**) Each control patient's TGF-β1 plasma level is depicted as a gray dot, with the line indicating the median. Each individual patient's TGF-β1 plasma level is depicted as a dot, with a line connecting each patient's 6- and 72-hour data. Those who had a decrease in TGF-β1 plasma are depicted in red. (**B**) Distribution of patient outcomes on the modified Rankin scale by TGF-β1 response. *n* = 22 controls and 22 ICH patients.

Using this dichotomy in TGF-β1 response, we explored the functional outcomes of patients at 90 days and found a marked shift toward improved outcomes in the patients who increased their circulating TGF-β1 levels by 72 hours after ICH (Figure 6B). In univariate analysis, an increase in TGF-β1 was associated with improved functional outcome, while other clinical variables were not associated with TGF-β1 response (Table 1). However, several of these variables have strong associations with functional outcome and had trends toward greater severity among the patients who had decreased TGF-β1. Clinically these have been combined into the ICH score (37), a prognostic scoring system that includes Glasgow coma scale score, age, infratentorial location, intraventricular hemorrhage, and volume of the hemorrhage. Therefore, a multivariable model was created adjusting for the impact of ICH score on functional outcomes. Patients who had an increase in plasma TGF-β1 concentrations from 6 to 72 hours had better outcomes by 90 days, independent of known predictors of clinical outcome (*n* = 22, Table 2). Thus, our data show that TGF-β1 is highly associated with functional recovery after ICH in patients.

Discussion

Under basal conditions, tissue-resident macrophages are seeded into their respective organs during development to maintain tissue homeostasis (13, 38–40). Thus, they are poised for immunosurveillance and to act as first responders to potential pathogens (39). Because of the robust infiltration of blood-derived macrophages during inflammation and the difficulties differentiating the cells in tissue, the specific role of tissue-resident macrophages in disease models of tissue injury is not well defined. Here, we show that microglia dramatically transition phenotypes within the first 2 weeks after ICH and that this transition is critical for functional recovery. We also show that TGF-β1 modulates the microglial phenotype and promotes functional recovery.

Microglia have dynamic changes in gene expression after ICH, expressing proinflammatory genes early after ICH before transitioning to a transcriptional program associated with tissue repair. Through transcriptional profiling, we identified the genes that contribute significantly to the temporal evolution of microglia phenotype. In the acute phase (day 1), microglia have a proinflammatory phenotype, yet this response was transient, as the majority

of genes that were upregulated on day 1 were already suppressed by day 7. Interestingly, when the entire gene set was clustered by time point, day 3 microglia clustered closest to the naive microglia. This was unexpected, as day 3 is the peak of peripheral leukocyte infiltration after ICH and considered to be the peak of the inflammatory response. These findings are reminiscent of findings in EAE, where at disease onset microglia upregulated chemokines but otherwise exhibited suppressed activation and metabolic phenotype compared with naive microglia (41). These similar findings may suggest that this phenomenon is conserved in microglia across various diseases.

In our model, microglia obtain a phenotype associated with recovery starting at day 7, which remains upregulated through day 28. The majority of the genes in these clusters were expressed in the naive state, decreased on days 1–3, and then recovered beginning at day 7 to reach levels higher than baseline by day 28. Included in this set are several genes associated with microglia, including *P2ry12*, *Tgfbr1*, *Cx3cr1*, and *Mertk*, suggesting that these genes are differentially regulated in the mouse during inflammation and may have roles in the resolution of inflammation. Overall, our work helps to identify gene pathways in the tissue-resident population of the CNS. By specifically studying microglia, we identified that TGF-β1 mediates the pathways involved in microglial recovery after ICH, a finding with potential therapeutic implications.

In recent years, microglial responses have been primarily dichotomized into two categories: classical, or proinflammatory, activation; and alternative activation, a phenotype associated with wound healing, tissue repair, and antiinflammatory properties (15, 42). Alternative activation has been attributed to IL-4 and IL-13 signaling on microglia (15). Microglia are often defined as alternatively activated through cell surface marker expression; YM1, FIZZ1, arginase 1, CD206, CD301, and CD163 are most commonly used to distinguish alternatively activated microglia from classically activated microglia. We did not observe significant changes over time in the transcription of conventional markers of alternative activation in microglia after ICH. Rather, our findings suggest that microglia transition to a phenotype that is a *type* of alternative activation that contributes to brain recovery, a phenotype that we would not have been able to define using traditional methods and markers. Consistent with our findings, TGF-β1 has been shown to

Table 1. Univariate analyses of the clinical cohort by TGF-β1 response

Variable	TGF-β1 increase	TGF-β1 decrease	P
Age (yr)	65 [59.2–69.2]	74.65 [59.05–78.5]	NS
Male sex	6 (46%)	6 (50%)	NS
ICH volume (ml)	9.1 [2.5–22.5]	12.4 [6.1–51.6]	NS
Intraventricular hemorrhage	5 (38%)	5 (42%)	NS
Infratentorial location	2 (15%)	0 (0%	NS
Initial GCS score	15 [14–15]	14 [13–15]	NS
ICH score	0 [0–1]	1.5 [1–2]	NS
Infection within 72 hours	1 (8%)	3 (25%)	NS
mRS at 90 days	2 [1.5–3]	4.5 [3–6]	< 0.01

NS: $P > 0.05$. Data presented as mean ± SD when data were normally distributed; median [interquartile range] when data were not normally distributed; and number (percentages). GCS, Glasgow coma scale; mRS, modified Rankin scale.

induce a form of alternative activation in macrophages (43, 44). Our data show that TGF-β1 drives microglial alternative activation in a clinically relevant in vivo model of disease.

The importance of TGF-β1 on microglia development and homeostasis and the role of TGF-β1 and TGFBR1 after different neurological disease have recently been reported (8, 45–47). *Tgfb1* and *Tgfbr1* gene expression are highly upregulated in WT microglia during the second week after ICH. We found that CX3CR1-null BM chimeras do not functionally recover after ICH and CX3CR1-null microglia have a significant reduction in *Tgfb1* gene expression. Our data suggest that microglial TGF-β1 is important in the microglial transition from proinflammatory to reparative after ICH. In vitro, TGF-β1 reduced microglial *Ccl2*, *Tnf*, and *Il6* gene expression and IL-6 secretion. In vivo, TGF-β1 treatment improved functional outcomes and decreased microglial IL-6 gene expression. It has recently been shown that *trans*-signaling of *Il6* through soluble IL-6R and transmembrane gp130 contributes to gliosis, blood-brain barrier breakdown, and neurodegeneration (48). This raises the possibility that the quelling of microglial IL-6 is critical in functional recovery after ICH; however, this requires further investigation. Interestingly, we were able to show that one dose of TGF-β1, when given after ICH in two separate models of ICH, improved functional outcomes that persisted, suggesting that TGF-β1 has a potentially long-lasting therapeutic effect.

Our work builds on evidence of the importance of TGF-β1 emerging from other CNS disease models. Silencing of TGF-BR1 on microglia promoted neuroinflammation and neuronal damage in a model of Parkinson's disease (46). However, early astrocyte production of TGF-β1 appears to establish a permissive environment for autoimmunity and enhanced inflammation in EAE (49). In a rat model of ischemic stroke, TGFBR1 was upregulated on microglia (47), although no functional role was investigated. Astrocyte signaling through TGF-β1 has been shown to limit neuroinflammation after experimental ischemic stroke. In Ast-Tbr2DN mice, which carry dominant negative mutant type II TGF-β receptor, inhibition of astrocytic TGF-β1 signaling led to a decrease in TGF-β1 levels in brain, enhanced inflammation, and impaired long term outcomes. However, effects on microglia phenotype were not assessed (50). While we did not assess astrocyte

phenotypes after ICH or find evidence that astrocytes respond to TGF-β1 at 14 days after ICH, it is possible that astrocytes provide the early source of TGF-β1 that initiates the phenotype modulation in microglia.

We used the CD45^{int}CD11b$^+$ classification of microglia in WT mice (51–53), which matched the high CX3CR1 expression in microglia from our BM chimeras and also was recently reported to closely match expression of the microglial marker TMEM119 (9). Our in vitro work relied on primary microglia, eliminating concerns about phenotypic differences observed in immortalized microglial cell lines (8). This provides a robust data set that furthers our understanding of microglial biology.

Interestingly, we also found that TGF-β1 response in patients is an independent predictor of patient outcome after ICH, which we believe to be a novel finding. The source of the TGF-β1 measured in ICH patients' plasma remains unclear. The murine time course of changes in the periphery match changes in the brain, suggesting that they are linked, perhaps due to breakdown of the blood brain barrier. It is likely that peripheral platelets, leukocytes, astrocytes, and microglia all contribute to the TGF-β1 concentrations measured in ICH patients' plasma. Taken together, our data show that microglia transition from a proinflammatory phenotype early after ICH into a phenotype that promotes wound healing and repair and that this occurs independent of IL-4 and IL-13 signaling. Our data indicate that TGF-β1 modulates microglia-mediated neuroinflammation after ICH and promotes functional recovery in both mice and humans.

Methods

Animals. Male B6.SJL-Ptprca Pep3b/BoyJ (CD45.1), C57/BL6J (WT), and B6.129P-Cx3cr1tm1Litt/J (*Cx3cr1$^{GFP/GFP}$* and *Cx3cr1$^{+/GFP}$*) mice were purchased from The Jackson Laboratory and then were bred in house. All mice were housed in standard conditions with a 12-hour light cycle, 22.2°C, and ad libitum access to food and water.

BM chimeras. To specifically study the role of microglial CX3CR1 after ICH, we made BM chimeras as previously described (54). Male WT and CX3CR1-null mice (congenically marked CD45.2) 6–8 weeks of age were irradiated with 12 Gy and reconstituted with BM from a WT donor congenically marked CD45.1, herein referred to as WT BM chimeras and CX3CR1-null BM chimeras. BM was allowed to engraft 8–10 weeks prior to ICH surgery. Percent chimerism was measured at 8 weeks after BM engraftment by flow cytometry. Successful chimerism was defined as the presence of at least 90% CD45.1$^+$ leukocytes.

Table 2. TGF-β1 response is independently associated with functional outcome at 90 days

Variable	OR	95% CI	P
TGF-β1 response	0.08	0.01–0.57	0.01
ICH score	2.99	1.33–6.69	0.008

Ordinal logistic regression model of TGF-β1 response and patient outcomes adjusted for the ICH score. An increase in TGF-β1 from 6 to 72 hours was independently associated with better functional outcome. $n = 22$. OR, odds ratio.

ICH surgery. Mice were anesthetized with 1%–5% isoflurane, and all efforts were made to minimize pain and suffering. For experiments using the blood injection model of ICH, ICH was induced by injection of 20–25 μl whole blood 2.5 mm lateral to bregma, 3 mm deep at a 5° angle as previously described (55). For experiments using BM chimeras, whole blood from a WT donor was used to create the hemorrhage. It has previously been shown that the cellular composition of the ICH impacts functional outcome and the inflammatory response in mice (56); therefore, WT blood was used to normalize the ICH components between genotypes. Chimeras were 13–15 weeks of age when ICH was induced. For experiments performed on WT mice, mice were 8–10 weeks of age when ICH was induced. We used the collagenase model of ICH, which results in the degradation of the vascular basement membrane ICH for confirmatory experiments. Briefly, ICH was induced by injection of 0.05 U type VII collagenase VII (from *Clostridium histolyticum*; Sigma-Aldrich) in 1 μl PBS at the same coordinates as the blood injection model.

TGF-β1 treatment. Mice were treated with 10 ng TGF-β1 or vehicle (PBS) in a final volume of 1 μl (45). Mice were randomized by coin flip into either TGF-β1 or PBS treatment groups. For behavioral experiments in which mice were pretreated, TGF-β1 or PBS was injected directly into the right striatum 10 minutes prior to ICH, at the same coordinates where ICH was induced. For experiments where mice were post-treated, TGF-β1 or PBS was delivered by intracerebroventricular (i.c.v.) injections 0.5 mm posterior and 0.75 mm lateral to bregma (57) 4 hours following ICH surgery.

Behavioral testing. Mice were behaviorally tested for up to 14 days after ICH to examine neurological deficits and functional recovery after ICH. All behavioral testing was performed by an observer blinded to genotype and treatment. Mice performed cylinder test 1, 3, 7, and 14 days after ICH as previously described (56). Briefly, mice were placed in a clear cylinder and allowed to freely rear for 20 rears, and the first forelimb placed was recorded. A laterality index was calculated [(right – left)/(right + left + both)], in which greater positive numbers indicate a more severe left hemiparesis (58). For the corner turn test, the mouse was allowed to proceed into a 30° corner and then freely turn either left or right to exit the corner. The choice of direction during 10 trials was recorded and the percentage of left turns was calculated. For beam walking test, mice were placed on a copper pipe suspended 40 cm above a table top at 1 or 14 days after ICH. Each mouse was given 5 trials to cross the beam and the furthest distance was recorded (59). Based on our experience in previous experiments, success on the test was defined as being able to walk a distance 20 cm or greater. For forced run test, mice were placed in an enclosed treadmill 14 days after ICH and forced to run at certain speeds (60). The top speed the mouse could run was recorded. Mice were tested only once on the beam walking test and forced run test to avoid learning effects.

Primary microglial cultures. Primary microglial cultures were created as previously described (61). Briefly, cortices were dissected from P0–P3 male, WT pups. Brains were dissociated using the neural dissociation kit with papain (Miltenyi Biotec) and the cell suspension was plated in T75 flasks in L929 media. Microglia were grown on an astrocyte bed for 2 weeks and then gently shaken off from the astrocyte layer. Supernatants containing the microglia were collected and spun down. Microglial purity was determined by flow cytometry (Supplemental Figure 7). Cells were counted and plated at 50,000 cells per well in DMEM media supplemented with 10% fetal bovine serum,

100 U/ml penicillin and 100 mg/ml streptomycin, and 30% L929 media (glial conditioned media; refs. 62, 63). Cells were allowed to rest for 4–5 days prior to use. Primary microglia were treated with 10 ng TGF and 10 U/ml thrombin for 8 or 24 hours in serum-free X-VIVO media (Lonza). Cells were harvested from plates using Accutase (Thermo Fisher Scientific) and used for quantitative RT-PCR (qRT-PCR) or intracellular cytokine staining.

Cell sorting for qRT-PCR and transcriptional analysis. Mice were sacrificed 0.5, 1, 3, 7, and 14 days after ICH and perfused with 40 ml cold PBS. Perihematomal brains were harvested and mechanically and enzymatically digested with DNase, dispase, and collagenase for 45 minutes at 37°C. Brains were then placed on a 30%/70% Percoll gradient to isolate leukocytes and remove myelin. Cells were washed and stained with antibodies for cell surface markers (CD45 [30-F11], Ly6C [HK1.4, eBiosciences], CD11b [M1/70], Ly6G [1A8, Tonbo Biosciences], CD3e [500A2, BD Biosciences]) for 20 minutes at room temperature. Microglia were identified as CD45^{int}CD11b^{+} cells for WT experiments and CD45.2^{int}CD11b^{+} cells for chimeric experiments, and were sorted on a FACSAria. The microglia population was confirmed by high CX3CR1 expression. RNA was extracted from sorted microglia and primary microglia using a commercially available kit (RNAqueous-Micro, Ambion). cDNA from sorted microglia was synthesized with Sensiscript reverse transcriptase (QIAGEN). RNA from primary microglia was extracted and cDNA synthesized using SuperScript IV (Life Technologies). qRT-PCR was performed using SYBR Green (QIAGEN) for the following genes: β-actin, *Tnf*, *Il6*, *Ccl2*, *Tgfbr1*, *Socs3*, *Bdnf*, *Cd206* (Supplemental Table 2), and *Tgfb1*. Cell culture samples were analyzed by normalizing gene of interest expression to β-actin. Sorted microglial samples for qRT-PCR were analyzed using the ΔΔCt method (64). In experiments for unbiased transcriptional analysis, three 4-mm perihematomal sections of brain were pooled per replicate and brains were processed as above. Microglia (CD45^{int}CD11b^{+}) were sorted, and cells were lysed in 4 μl RLT buffer (QIAGEN) and 10 μl RNA samples directly hybridized with a pool of 780 capture probes; gene expression was analyzed by nCounter Digital Analyzer according to the manufacturer's instructions (NanoString Technologies). The gene expression was normalized to positive controls and housekeeping genes and calculated as relative counts.

Transcriptional analysis. NanoString data were preprocessed according to the manufacturer's instructions and then further analyzed using custom MATLAB scripts. Briefly, nCounter data were normalized to housekeeping genes, and genes with expression below the threshold of detection at all time points were eliminated. Resulting nCounter data were imported into MATLAB and *Z* score normalized. To remove genes that did not significantly change over time, two MATLAB functions were used: genevarfilter and geneentropyfilter. The former removes genes that have a variance above a specified percentile, where variance is calculated for each gene profile. The latter removes genes whose profile is low entropy overall. The remaining genes were clustered hierarchically to identify 15 clusters of genes based on coloring the dendrogram (distance of 6).

To identify genes driving change over time, PCA was performed, and results were presented as a biplot. In order to find genes that contribute "the most," a circle was drawn whose radius was the average of the 90th percentile of the magnitude of the principal component coefficients. The goal of using this circle was to allow for consistent identification of genes. Genes whose projections were on or outside this

circle were labeled on the plot, and each sample was plotted and color coded. Heatmaps were created using MATLAB and GENE-E, a matrix visualization software available through the Broad Institute (http://www.broadinstitute.org). Enrichment analysis was performed using the Cytoscape (v3.3.0) plugin GeneMania (v3.4.0). Genes appearing in the lower-left quadrant of our PCA were used for GeneMANIA analysis with the following network interactions: coexpression, pathway, physical interaction, and shared protein domains. GO biological process–based weighting was used.

Intracellular staining for cytokine phosphorylation status by flow cytometry. To measure pSMAD2/3, primary microglia were stimulated with 10 U/ml thrombin with and without 10 ng TGF-β1 for 20 minutes prior to fixation with 4% paraformaldehyde. Cells were permeabilized with ice-cold methanol for a minimum of 20 minutes on ice. Cells were then stained for CD45 (30-F11, eBioscience), CD11b (M1/70, Tonbo Biosciences), and pSMAD2/3 (O72-670, BD Biosciences). To measure pSTAT6 in perihematomal regions, mice were sacrificed at 7 days and samples were prepared as described above. Cells were stained for CD45 (30-F11, eBioscience), CD11b (M1/70, Tonbo Biosciences), CD3e (500A2, BD Biosciences), Ly6C (HK1.4, eBiosciences), and pSTAT6 (J71-773.58.11, BD Biosciences). For measuring TNF production, primary microglia were treated for 8 hours as described above with the presence of Brefeldin A for 5 hours. Cells were washed from Accutase with PBS and then stained with antibodies to cell surface markers CD45 (30-F11, eBioscience) and CD11b (M1/70, Tonbo Biosciences) for 20 minutes at room temperature. Cells were fixed (BD CytoFix/CytoPerm) for 20 minutes at 4°C prior to being permeabilized and stained with antibodies to intracellular TNF (MP6-XT22, BioLegend) for 30 minutes at 4°C. Cells were run on a BD LSRFortessa.

ELISA and multiplex. Perihematomal brains were harvested from naive mice and mice 1, 3, 7, 10, and 14 days after ICH and hemisphere were separated. Hemispheres were homogenized using 1mm glass beads in RIPA buffer (Cell Signaling Technology) containing phosphatase and protease inhibitors (Roche) in a bead beater. Samples were spun at 8,000 relative centrifugal force (rcf) for 30 seconds to remove bubbles, sonicated, and spun at 14,000 rcf for 15 minutes. BCA assay was performed to quantify total amount of protein in each hemisphere. Eighty micrograms of brain tissue was plated per well. For ELISA on cell supernatants, supernatants were harvested from cells stimulated for 24 hours. Ten microliters of supernatants were loaded per well for TNF and IL-6, and 50 μl cell supernatants were loaded per well for BDNF ELISAs. IL-6, CCL2, IL-10, IL-13, IL-17, and IL-4 concentrations were measured by multiplex ELISA (Millipore). TGF-β1 (eBioscience) and BDNF (Promega) concentrations were measured using commercially available kits. For mouse serum TGF-β1 levels, 100 μl blood was collected by cardiac puncture at sacrifice and allowed to clot on ice for 20 minutes then spun at 2000 g for 10 minutes. Supernatants were collected and frozen at –80°C until analysis. Samples for TGF-β1 and BDNF ELISAs were acidified with 1N HCl for 10 minutes, then neutralized with 1N NaOH prior to performing the ELISAs.

Immunofluorescence. Mice were sacrificed at 7 and 14 days after ICH and transcardially perfused with 20 ml PBS followed by 20 ml 4% paraformaldehyde. Brains were then harvested and post-fixed in 4% paraformaldehyde overnight at 4°C. Brains were then submerged in 30% sucrose for 48 hours and embedded in OCT. Seven-micrometer sections were cut and blocked with 2% normal goat serum for 1 hour at room temperature. Samples were stained with primary antibodies

for CD11b (purified and biotinylated forms used; eBioscience, 1:300) and pSMAD2 (Millipore, 1:500). Slides were washed twice and then stained with secondary antibodies goat anti-rat–Cy3 and goat anti-rabbit–DyLight 488 (Life Technologies, 1:500). Nuclei were stained with DAPI. Photographs were taken on a Leica DMi8 using the provided Leica LAS X software. Adjustments we made using the LAS X software. Sections were analyzed by an observer blinded to genotype.

Iron staining. DAB-enhanced Perls' staining was used to detect iron accumulation. Briefly, sections from PBS- and TGF-β1–injected brain tissue were washed with PBS and incubated in freshly prepared Perls' solution (5% potassium ferrocyanide/10% hydrochloric acid) for 30 minutes, followed by 5 PBS washes. After DAB incubation for 1.5 minutes and hematoxylin counterstaining, iron deposition in the perihemorrhagic area was digitized by microscope. Iron-positive cells were counted from 4 high-powered fields/mouse by an observer blinded to treatment.

Statistics: murine data. Based on means and standard errors of cylinder testing from prior work, an $n = 8$ is required to achieve 80% power to detect a 25% difference in laterality between groups at $\alpha = 0.05$ (65). Cylinder testing performed at multiple time points was evaluated by repeated measures ANOVA. Top running speed was evaluated by Wilcoxon rank sum test since the distribution was non-normal. Beam walk test was analyzed by χ^2 test. Analysis of intracellular staining, primary cell culture gene expression, and ELISA were measured by ANOVA followed by Tukey's post hoc test. Cell sorted microglial gene expression and percent of pSMAD$^+$CD11b$^+$ cells from IHC images was analyzed by Student's t test.

Patient cohort study. Patients were prospectively enrolled from Hartford Hospital (2010 to 2013) and the Hospital of the University of Pennsylvania (2008 to 2011). Blood was collected by peripheral venipuncture into lithium heparin tubes at 6 ± 6 hours and 72 ± 6 hours after ICH symptom onset (or last known well) and centrifuged at 2000 g for 10 minutes. Plasma was collected and then centrifuged at 15,000 g to remove residual platelets and the supernatant frozen at –80°C until analysis. Clinical data — including age, sex, volume of ICH, presence of intraventricular hemorrhage, location of ICH, initial Glasgow coma scale score, infections, surgical interventions, length of hospitalization, and functional outcomes — were prospectively collected. Functional outcomes were quantified using the modified Rankin scale score determined by a trained member of the Stroke teams at each hospital during a clinic visit or structured telephone interview. Control patients were identified from the Hartford Hospital outpatient cardiology clinic and from inpatients admitted to the Hartford Hospital stroke service with negative brain MRI scans (stroke mimics).

Statistics analysis: human data. Variables were tested for normality and reported as mean ± SD (if normal), median [interquartile range] (if skewed), or number (%). TGF-β1 levels were non-normally distributed. Patients were dichotomized by whether there was an increase or decrease in TGF-β1 levels between the two time points a priori based on the results of the murine studies. Univariate analyses were conducted to detect differences in clinical variables between the groups by Student's t test, Fisher's exact test, or Mann-Whitney U test, as appropriate. A multivariable model was created to determine the independent association of TGF-β1 response with functional disability at 90 days by ordered logistical regression while adjusting for the ICH score. The proportional odds assumption was checked and upheld. All statistical analyses were performed using Stata v11.

Author contributions

RAT designed, conceived, and performed experiments and wrote the manuscript. CFC, MDH, BMG, AS, YA, and SCR performed some experiments. MHA edited the manuscript. BAG and JCL analyzed transcriptional data and edited the manuscript. LDM, MTM, SEK, and LHS supervised patient cohort study and edited the manuscript. DAH provided conceptual advice and edited the manuscript. LHS supervised all studies and edited the manuscript. All authors discussed the results and approved the manuscript.

Acknowledgments

Address correspondence to: Lauren H. Sansing, Yale University School of Medicine, 300 George Street, Suite 353, New Haven, Connecticut 06511, USA. Phone: 203.737.4802; E-mail: lauren.sansing@yale.edu.

MDH's present address is: RA Capital Management, Boston, Massachusetts, USA.

1. Manno EM. Update on intracerebral hemorrhage. *Continuum (Minneap Minn)*. 2012;18(3):598–610.
2. Qureshi AI, Mendelow AD, Hanley DF. Intracerebral haemorrhage. *Lancet*. 2009;373(9675):1632–1644.
3. Keep RF, Hua Y, Xi G. Intracerebral haemorrhage: mechanisms of injury and therapeutic targets. *Lancet Neurol*. 2012;11(8):720–731.
4. Zhao X, et al. Hematoma resolution as a target for intracerebral hemorrhage treatment: role for peroxisome proliferator-activated receptor gamma in microglia/macrophages. *Ann Neurol*. 2007;61(4):352–362.
5. Schulz C, et al. A lineage of myeloid cells independent of Myb and hematopoietic stem cells. *Science*. 2012;336(6077):86–90.
6. Hoeffel G, et al. C-Myb(+) erythro-myeloid progenitor-derived fetal monocytes give rise to adult tissue-resident macrophages. *Immunity*. 2015;42(4):665–678.
7. Kierdorf K, et al. Microglia emerge from erythro-myeloid precursors via Pu.1- and Irf8-dependent pathways. *Nat Neurosci*. 2013;16(3):273–280.
8. Butovsky O, et al. Identification of a unique TGF-β-dependent molecular and functional signature in microglia. *Nat Neurosci*. 2014;17(1):131–143.
9. Bennett ML, et al. New tools for studying microglia in the mouse and human CNS. *Proc Natl Acad Sci U S A*. 2016;113(12):E1738–E1746.
10. Dey A, Allen J, Hankey-Giblin PA. Ontogeny and polarization of macrophages in inflammation: blood monocytes versus tissue macrophages. *Front Immunol*. 2014;5:683.
11. Paolicelli RC, et al. Synaptic pruning by microglia is necessary for normal brain development. *Science*. 2011;333(6048):1456–1458.
12. Mantovani A, Biswas SK, Galdiero MR, Sica A, Locati M. Macrophage plasticity and polarization in tissue repair and remodelling. *J Pathol*. 2013;229(2):176–185.
13. Davies LC, Jenkins SJ, Allen JE, Taylor PR. Tissue-resident macrophages. *Nat Immunol*. 2013;14(10):986–995.
14. Wang J. Preclinical and clinical research on inflammation after intracerebral hemorrhage. *Prog Neurobiol*. 2010;92(4):463–477.
15. Starossom SC, et al. Galectin-1 deactivates classically activated microglia and protects from inflammation-induced neurodegeneration. *Immunity*. 2012;37(2):249–263.
16. Sica A, Mantovani A. Macrophage plasticity and polarization: in vivo veritas. *J Clin Invest*. 2012;122(3):787–795.
17. Cherry JD, Olschowka JA, O'Banion MK. Neuroinflammation and M2 microglia: the good, the bad, and the inflamed. *J Neuroinflammation*. 2014;11:98.
18. Ponomarev ED, Maresz K, Tan Y, Dittel BN. CNS-derived interleukin-4 is essential for the regulation of autoimmune inflammation and induces a state of alternative activation in microglial cells. *J Neurosci*. 2007;27(40):10714–10721.
19. Liu X, et al. Interleukin-4 is essential for microglia/macrophage M2 polarization and long-term recovery after cerebral ischemia. *Stroke*. 2016;47(2):498–504.
20. Wynn TA, Vannella KM. Macrophages in tissue repair, regeneration, and fibrosis. *Immunity*. 2016;44(3):450–462.
21. Qin H, Wilson CA, Roberts KL, Baker BJ, Zhao X, Benveniste EN. IL-10 inhibits lipopolysaccharide-induced CD40 gene expression through induction of suppressor of cytokine signaling-3. *J Immunol*. 2006;177(11):7761–7771.
22. de Bilbao F, et al. In vivo over-expression of interleukin-10 increases resistance to focal brain ischemia in mice. *J Neurochem*. 2009;110(1):12–22.
23. Tsunawaki S, Sporn M, Ding A, Nathan C. Deactivation of macrophages by transforming growth factor-beta. *Nature*. 1988;334(6179):260–262.
24. Bonniaud P, et al. Smad3 null mice develop airspace enlargement and are resistant to TGF-beta-mediated pulmonary fibrosis. *J Immunol*. 2004;173(3):2099–2108.
25. Eyo UB, Dailey ME. Microglia: key elements in neural development, plasticity, and pathology. *J Neuroimmune Pharmacol*. 2013;8(3):494–509.
26. Abutbul S, et al. TGF-β signaling through SMAD2/3 induces the quiescent microglial phenotype within the CNS environment. *Glia*. 2012;60(7):1160–1171.
27. Jung S, et al. Analysis of fractalkine receptor CX(3)CR1 function by targeted deletion and green fluorescent protein reporter gene insertion. *Mol Cell Biol*. 2000;20(11):4106–4114.
28. Chapman GA, Moores K, Harrison D, Campbell CA, Stewart BR, Strijbos PJ. Fractalkine cleavage from neuronal membranes represents an acute event in the inflammatory response to excitotoxic brain damage. *J Neurosci*. 2000;20(15):RC87.
29. Harrison JK, et al. Role for neuronally derived fractalkine in mediating interactions between neurons and CX3CR1-expressing microglia. *Proc Natl Acad Sci U S A*. 1998;95(18):10896–10901.
30. Cardona AE, et al. Control of microglial neurotoxicity by the fractalkine receptor. *Nat Neurosci*. 2006;9(7):917–924.
31. Corona AW, et al. Fractalkine receptor (CX3CR1) deficiency sensitizes mice to the behavioral changes induced by lipopolysaccharide. *J Neuroinflammation*. 2010;7:93.
32. Ginhoux F, Lim S, Hoeffel G, Low D, Huber T. Origin and differentiation of microglia. *Front Cell Neurosci*. 2013;7:45.
33. Hu S, Xi G, Jin H, He Y, Keep RF, Hua Y. Thrombin-induced autophagy: a potential role in intracerebral hemorrhage. *Brain Res*. 2011;1424:60–66.
34. Hua Y, Keep RF, Hoff JT, Xi G. Brain injury after intracerebral hemorrhage: the role of thrombin and iron. *Stroke*. 2007;38(2 Suppl):759–762.
35. Banks JL, Marotta CA. Outcomes validity and reliability of the modified Rankin scale: implications for stroke clinical trials: a literature review and synthesis. *Stroke*. 2007;38(3):1091–1096.
36. Rankin J. Cerebral vascular accidents in patients over the age of 60. II. Prognosis. *Scott Med J*. 1957;2(5):200–215.
37. Hemphill JC, Bonovich DC, Besmertis L, Manley GT, Johnston SC. The ICH score: a simple, reliable grading scale for intracerebral hemorrhage. *Stroke*. 2001;32(4):891–897.
38. Ginhoux F, et al. Fate mapping analysis reveals that adult microglia derive from primitive macrophages. *Science*. 2010;330(6005):841–845.
39. Ginhoux F, Guilliams M. Tissue-resident macrophage ontogeny and homeostasis. *Immunity*. 2016;44(3):439–449.
40. Gomez Perdiguero E, et al. Tissue-resident macrophages originate from yolk-sac-derived erythro-myeloid progenitors. *Nature*. 2015;518(7540):547–551.

41. Yamasaki R, et al. Differential roles of microglia and monocytes in the inflamed central nervous system. *J Exp Med*. 2014;211(8):1533–1549.

42. Ajmone-Cat MA, Mancini M, De Simone R, Cilli P, Minghetti L. Microglial polarization and plasticity: evidence from organotypic hippocampal slice cultures. *Glia*. 2013;61(10):1698–1711.

43. Gong D, Shi W, Yi SJ, Chen H, Groffen J, Heisterkamp N. TGFβ signaling plays a critical role in promoting alternative macrophage activation. *BMC Immunol*. 2012;13:31.

44. Gordon S. Alternative activation of macrophages. *Nat Rev Immunol*. 2003;3(1):23–35.

45. Norden DM, Fenn AM, Dugan A, Godbout JP. TGFβ produced by IL-10 redirected astrocytes attenuates microglial activation. *Glia*. 2014;62(6):881–895.

46. Liu Z, Chen HQ, Huang Y, Qiu YH, Peng YP. Transforming growth factor-β1 acts via TβR-I on microglia to protect against MPP(+)-induced dopaminergic neuronal loss. *Brain Behav Immun*. 2016;51:131–143.

47. Pál G, Lovas G, Dobolyi A. Induction of transforming growth factor beta receptors following focal ischemia in the rat brain. *PLoS One*. 2014;9(9):e106544.

48. Campbell IL, et al. Trans-signaling is a dominant mechanism for the pathogenic actions of interleukin-6 in the brain. *J Neurosci*. 2014;34(7):2503–2513.

49. Luo J, et al. Glia-dependent TGF-beta signaling, acting independently of the TH17 pathway, is critical for initiation of murine autoimmune encephalomyelitis. *J Clin Invest*. 2007;117(11):3306–3315.

50. Cekanaviciute E, Fathali N, Doyle KP, Williams AM, Han J, Buckwalter MS. Astrocytic transforming growth factor-beta signaling reduces subacute neuroinflammation after stroke in mice. *Glia*. 2014;62(8):1227–1240.

51. Hickman SE, et al. The microglial sensome revealed by direct RNA sequencing. *Nat Neurosci*. 2013;16(12):1896–1905.

52. Campanella M, Sciorati C, Tarozzo G, Beltramo M. Flow cytometric analysis of inflammatory cells in ischemic rat brain. *Stroke*. 2002;33(2):586–592.

53. Cardona AE, Huang D, Sasse ME, Ransohoff RM. Isolation of murine microglial cells for RNA analysis or flow cytometry. *Nat Protoc*. 2006;1(4):1947–1951.

54. Schluns KS, Nowak EC, Cabrera-Hernandez A, Puddington L, Lefrançois L, Aguila HL. Distinct cell types control lymphoid subset development by means of IL-15 and IL-15 receptor alpha expression. *Proc Natl Acad Sci U S A*. 2004;101(15):5616–5621.

55. Sansing L, Kasner S, McCullough L, Agarwal P, Welsh F, Kariko K. Autologous blood injection to model spontaneous intracerebral hemorrhage in mice. *J Vis Exp*. 2011;(54):e2618.

56. Sansing LH, Harris TH, Welsh FA, Kasner SE, Hunter CA, Kariko K. Toll-like receptor 4 contributes to poor outcome after intracerebral hemorrhage. *Ann Neurol*. 2011;70(4):646–656.

57. Zhu W, Gao Y, Chang CF, Wan JR, Zhu SS, Wang J. Mouse models of intracerebral hemorrhage in ventricle, cortex, and hippocampus by injections of autologous blood or collagenase. *PLoS One*.

2014;9(5):e97423.

58. Li X, Blizzard KK, Zeng Z, DeVries AC, Hurn PD, McCullough LD. Chronic behavioral testing after focal ischemia in the mouse: functional recovery and the effects of gender. *Exp Neurol*. 2004;187(1):94–104.

59. Thal SC, Mebmer K, Schmid-Elsaesser R, Zausinger S. Neurological impairment in rats after subarachnoid hemorrhage--a comparison of functional tests. *J Neurol Sci*. 2008;268(1–2):150–159.

60. Hetze S, Römer C, Teufelhart C, Meisel A, Engel O. Gait analysis as a method for assessing neurological outcome in a mouse model of stroke. *J Neurosci Methods*. 2012;206(1):7–14.

61. Ijichi K, et al. MMP-3 mediates psychosine-induced globoid cell formation: implications for leukodystrophy pathology. *Glia*. 2013;61(5):765–777.

62. Devarajan G, Chen M, Muckersie E, Xu H. Culture and characterization of microglia from the adult murine retina. *ScientificWorldJournal*. 2014;2014:894368.

63. Regen T, et al. CD14 and TRIF govern distinct responsiveness and responses in mouse microglial TLR4 challenges by structural variants of LPS. *Brain Behav Immun*. 2011;25(5):957–970.

64. Livak KJ, Schmittgen TD. Analysis of relative gene expression data using real-time quantitative PCR and the 2(-Delta Delta C(T)) Method. *Methods*. 2001;25(4):402–408.

65. Taylor RA, Hammond MD, Ai Y, Sansing LH. CX3CR1 signaling on monocytes is dispensable after intracerebral hemorrhage. *PLoS One*. 2014;9(12):e114472.